Journal of Fluorescence, Vol. 7, No. 1, 1997

Frequency-Domain Lifetime Imaging Methods at Unilever Research

John J. Birmingham[1]

Received June 14, 1996; accepted September 25, 1996

Fluorescence lifetime imaging methodology has been successfully implemented at Unilever Research in a frequency-domain manner. The experimental rig constructed comprises a wide-bandwidth electrooptic modulator operating on a CW argon-ion laser. The modulated excitation with a typical upper modulation frequency limit of 200 MHz falls on macroscopic samples and the resultant scattered light or fluorescence emission is then imaged onto a custom gain-modulatable image intensifier and slow-scan CCD camera combination. Phase adjustment of the image intensifier relative to the laser modulator is achieved by the RF function generator driving the intensifier. Both homodyne and heterodyne (500-Hz) strobing modes are employed to generate a double image stack (scattered light reference and fluorescence emission) comprising an image sequence as a function of instrumental phase difference. These image stacks are analyzed by Fourier least-squares methods to yield lifetime images by both phase delay and normalized demodulation. Correct operation of the apparatus is deduced from the direct imaging of a quencher-induced lifetime variation of BODIPY disulfonate over a range of concentrations. A typical industrially relevant sample, comprising an investigation of the lifetime aspects of human dental enamel autofluorescence at 50-MHz modulation frequency, is given. This shows that there are real emission lifetime decreases of about 0.5 nsec in white-spot lesion areas compared to the surrounding sound enamel.

KEY WORDS: Image intensifier; direct modulation; lifetime quenching; enamel autofluorescence; white-spot lesions.

INTRODUCTION

The ability to detect the fundamental event in the fluorescence emission process, that is, the rate of production of light, in a spatially resolved or imaging manner has developed rapidly in recent years. Imaging devices which are capable either of rapidly shuttering on the nanosecond time scale or of sinusoidally gain modulating at high frequencies form the core new devices on which modern fluorescence lifetime imaging (FLIM) methods depend. The ability with these devices to strobe the very fast decay kinetics allows high-quality low-light level imaging then to be performed with high-dynamic range cooled slow-scan charge-coupled device (CCD) cameras, for example. The frequency-domain techniques employing sinusoidally modulated excitation and synchronous image modulation with such image intensifier devices were first described by a number of groups in the early 1990s.[1-6] Time-domain techniques have also been successfully employed, with a growing emphasis on confocal laser scanning FLIM variants being apparent.[7-10] Two-photon time-resolved methods offering intrinsic optical sectioning capability have also been described.[11,12] FLIM methods such as these have been used to image experimental variables such as pH,[13,14] *p*Ca,[15,16] and NADH.[17] The key benefit of FLIM techniques lies in the ability to put all pixels of a classical

[1] Unilever Research, Port Sunlight Laboratory, Quarry Road East, Bebington, Wirral, Merseyside L63 3JW, U.K.

1053-0509/97/0300-0045$12.50/0

steady-state fluorescence image onto a correct quantitative footing, that is, to correct for any spatially variable dynamic quenching effects. By imaging the core clock of the process, the experimenter can now directly compare steady-state intensities measured at any two locations in an image and correct for any such effects. Apart from such correction procedures, FLIM offers a way of imaging the causes of lifetime variation, be they specific variables such as pH, pO_2, and pCa, or general factors such as polarity or fluidity, in an intensity-independent manner. Specific interactions between chromophores resulting in resonance energy transfer, for example, may also be best imaged in a quantitative manner by lifetime imaging techniques.

In an industrial context, the advantages of fluorescence emission in simultaneously offering sensitivity, selectivity, imaging capability over a wide range of distance scales, and the opportunity of imaging important microenvironmental variables such as pH and pO_2 are very attractive. However, the structural and compositional heterogeneity of systems in which fluorescence labels reporting on such variables may have to be deployed makes lifetime imaging methods very necessary. Accordingly, this paper describes the efforts at Unilever Research to construct a general FLIM capability. Because of the simplified data analysis methods possible with frequency-domain methods, these were chosen as a general approach in comparison to the time-domain methods.

EXPERIMENTAL METHODS

The instrumentation assembled for the FLIM apparatus is as follows. A Lexel-85 water-cooled argon-ion CW laser, operating at 488 nm and about 50-mW power, is sinusoidally intensity modulated by an external electrooptic modulator, specifically a wide-aperture KDP double-crystal Pockels cell of bandwidth 450 MHz (ISS Inc., IL). The modulated laser beam then passes through a stepper motor-driven half-wave plate and fixed prism polarizer combination, to provide convenient intensity control independent of the modulator, before being focused by a 4-in.-focal length fused silica lens into a liquid light guide (2 m long, Dolan–Jenner, MA). The light guide passes through a homemade "wiggler," consisting of an enclosed loudspeaker coil driven at 350 Hz, to randomize the laser speckle pattern across the sample. A high-speed avalanche silicon photodiode (Model C30998-350; EG&G Canada Ltd.), connected directly to a LeCroy-9400 digital storage oscilloscope, is used to measure the excitation modulation depth. Additionally, a standard side-window photomultiplier tube (Model 9781R; Thorn-EMI, Middlesex, UK) is used to monitor continually the steady-state excitation levels during the image sequence, using a quartz coverslip reflection off the main beam prior to fiber-optic launch. The sample end of the fiber optic terminates in a standard collimating head (Model 77644; Oriel Corp., CT) illuminating the macroscopic samples in a light-tight blacked enclosure from one side only at a 45° angle. The roof of the sample enclosure is bellows-connected through a computer-driven filter changer with two positions (laser line interference filter for scattered light reference images, Schott KV550 low-fluorescence long-pass filter for fluorescence emission images) to a flexible long-working distance macroscope lens system (Model MRM in basic configuration from Infinity Photo-Optical, CO). This imaging lens system focuses the sample images through a standard Olympus trinocular viewing head onto the final imaging detectors. These comprise a custom 18-mm-diameter GEN-II microchannel plate-based image intensifier (Code P8743-AM; EEV Ltd., Essex UK) relay lens coupled to a three-stage Peltier cooled slow-scan CCD camera (AT1 System, using EEV chip 578 × 385 pixels, 16 bit/pixel; Wrights Instruments, Middlesex, UK). The image intensifier has a quartz input window, an S25-type photocathode response, and a P20-type output phosphor. It offers both conventional pulse gating (5 ns) at the photocathode gating point and wide-bandwidth (220-MHz minimum) gain modulation on the main microchannel plate acceleration voltage point. About 50 V_{rms} driving voltage is required for adequate image modulation depths to be achieved, and the dual modulation facilities offered allow for both homodyne and heterodyne FLIM modes.

The driving electronics comprise a low-phase noise master 10-MHz oscillator (Model SG10; Stanford Research, CA), acting as external reference for two RF generators. The first of these is a Hewlett–Packard 1-GHz generator, Model 8656B, driving the image intensifier through a 43-dB wideband RF power amplifier (Model R1222CC; RF Power Labs Inc.; range, 0.1–220 MHz). The laser modulator is driven from a second signal generator (Model PSG1000; Farnell Ltd., West Yorkshire UK) through a 25-W linear RF amplifier (Model 525LA; ENI Ltd., New York; range, 0.5–500 MHz). The HP8656B generator has the capability of shifting the phase of its synthesized carrier frequency in 1° increments either positive or negative with respect to the external reference clock in a fully IEEE-programmable way. Although mostly homodyne FLIM methods are used for the work described in this paper, a heterodyne mode offers a quick "live" self-scanning way of view-

ing the overall image modulation depth. For such checks, the final CCD camera is replaced by any standard photomultiplier tube detector and the two generators augmented by a LeCroy-9100 arbitrary waveform generator externally clocked by the 10-MHz master oscillator. This allows us to generate an electrical sync signal at the heterodyne difference frequency of typically 500 Hz, and this then acts as reference input of a dual-phase lockin amplifier (Model 530, Stanford Research). The overall instrumental modulation depth and phase situation can then be directly read off the lock-in amplifier displays.

BODIPY disulfonate was obtained from Molecular Probes Inc. (Eugene, OR); potassium iodide quencher was from Aldrich Chemical Co. (Dorset, UK). Human premolar teeth were donated by dental surgeries to Unilever Research, these teeth being extracted not for the purposes of the FLIM experiments but for orthodontic reasons. The teeth were cleaned and sterilized before handling.

Data Analysis

A typical FLIM homodyne experiment performed with the equipment described above consists of two image stacks, one for the reference scattered light and the other for the fluorescence emission from the same sample. Each image stack consists of 60 CCD images acquired at a set of equispaced instrumental phase settings spanning 360° of the modulation frequency in use. Because the signal intensities are very different in the two image stacks, very different image integration times are necessary notwithstanding strong suppression of the excitation energy by means of the crossed polariser intensity control in the scattered light image stack. Therefore, the experiment is performed strictly serially rather than in an interleaved fashion, i.e., acquire fluorescent set, then wind back the instrumental phase to starting phase position and then acquire the reference image stack. These two stacks (about 60-MB total) are then transferred to a Silicon Graphics workstation (Indy Model; 100-MHz clock, 32-MB RAM) for data analysis. The core FLIM procedure is a Fourier least-squares analysis across each stack to give the dc level, ac amplitude, and phase (relative to initial instrumental phase setting) for each pixel. The software is written using PV-Wave scientific visualization and analysis environment (Visual Numerics Inc., CO), and because of the extensive matrix calculation modes available, no individual pixel-by-pixel loops per image per stack are in fact required. Thus the calculations are relatively fast and efficient; a single stack of 60 × 578 × 385 pixels takes just 40 s to reduce in this fashion. The results of each stack are then combined to yield the phase delay image and normalised demodulation images (fluorescence relative to scattered light). These are then converted to lifetime images assuming that the simplest single-component emission lifetime model is valid. If the lifetime images derived from the phase delay and normalized demodulation images are different, this is taken as an indication that a more complex decay model is in fact required. The Fourier analysis is general enough to allow for any stack image range, not just an integer number of periods, a minimum of three images per stack obviously being required. The excitation dc intensity monitor values are used to normalize each image in each stack prior to Fourier analysis, to obtain optimum sinewave shapes per pixel. The software also allows for regions with less than a user-specified steady-state intensity threshold to be set to zero in the time-resolved images, so that very weak pixels do not interfere with the display scaling for the lifetime images.

Overall Instrumental Performance

Figure 1 (top) shows the periodic output of the overall homodyne experiment at 50-MHz modulation frequency. Here only the central pixel intensity of the image field is read out as a function of time as the image intensifier function generator is phase scanned with respect to the modulator driving waveform, three full periods being requested in this case. The electrooptic modulator modulation depth was 70%, using the photodiode/oscilloscope direct monitoring. The overall homodyne modulation depth seen at 50 MHz is about 25%, implying that the image intensifier modulation depth must also be about 70% at this modulation frequency. The overall image intensifier dc gain voltage in this case was 500 V. This excellent performance falls off somewhat as the modulation frequency is increased to 200 MHz, the waveform depicted in Fig. 1 (bottom). The modulator modulation depth has decreased to 60%, and the overall homodyne modulation depth is now about 13%. This implies an image intensifier modulation depth at 200 MHz of about 44%. It is expected that the intensifier driving amplifier will have started to fall off at this frequency in any case, so we feel that the overall electrooptic performance of the EEV image intensifier is, for all practical purposes, excellent.

Figure 2 shows a typical phase calibration plot when a heterodyne (500-Hz) lock-in amplifier experiment is performed. The relationship between measured phase and requested phase delay is almost-perfect, with a slope very close to −1.0. However, because of the

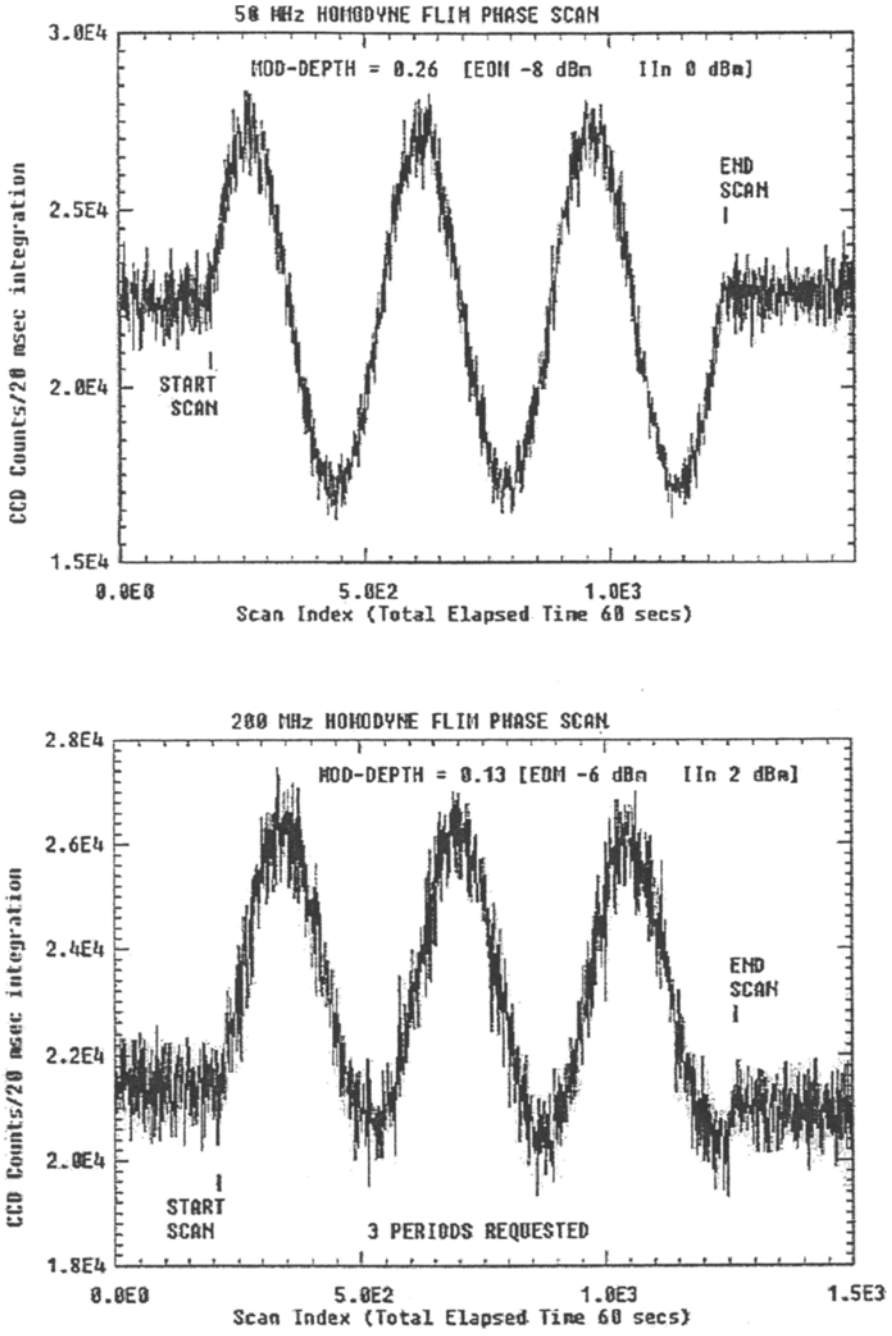

Fig. 1. Homodyne dynamic range measurements as the central pixel of the CCD camera is read out as a function of time as three periods of phase adjustment are performed by the image intensifier function generator. The start and stop points of the phase scan are indicated. The top panel is for a 50-MHz, and the bottom panel is for a 200-MHz modulation frequency. The signal generator drive voltages (dBm) are given. EOM, electro optic modulator; IIn, image intensifier levels.

serial nature of the experiment, in that first the fluorescence stack, then the scattered light reference stacks, is measured, the reproducibility of the intercept values (initial instrumental phase value) is of obvious importance. Performing the experiment in Fig. 2 repeatedly (10 trials), we measure an intercept phase value standard deviation of 0.27° at 50 MHz. Thus this amount of phase jitter will be present on both the average phase values

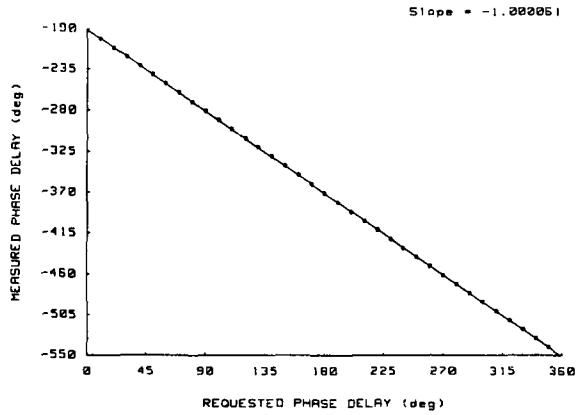

Fig. 2. Phase calibration scan at a 50-MHz modulation frequency during one period of phase delay adjustment. A photomultiplier tube and lock-in amplifier combination is used in place of an imaging detector to measure the phase during a heterodyne (500-Hz) experiment. Phase wraparounds at the half-period point have been removed before data plotting.

at a typical pixel for both fluorescence and reference situations. In lifetime terms, suppose that the sample gives a 50% full-scale phase delay at 50 MHz, i.e., 45° or a lifetime of 3.2 ns. With a phase jitter of 0.27°, this will give a lifetime spread of about 120 ps, or just under 4% lifetime error, allowing for 2 SD about the central phase peak in each stack. Faster lifetimes will have larger percentage errors than this, but slower lifetimes will be correspondingly less.

Imaging Performance

To quantify the overall lifetime imaging performance, a very simple sample comprising a sheet of standard graph paper is used as a scattered light target. Such an object is flat and offers a convenient regular gradation of scattered light intensities. The expected time-resolved result is that the modulation ratio and phase scattered light images should be flat and featureless, independent of the structure (dc intensity) of the object. Figure 3 shows the steady-state (DC), modulation depth (MOD), and phase images (PHASE) from such an object using scattered light only at 50-MHz (left column of images) and at 200-MHz modulation frequency (right column of images). Note that because the image intensifier geometry is circular and lens-relayed onto the rectangular format of the CCD chip, the four corners of the images are not active in imaging. Line A,B denotes the illumination axis of the experiment, B being the side nearest the fiber-optic delivery point. The time-resolved images at 50 MHz are almost-featureless as expected, but there is a slight gradient (about 2°) in measured phase values as we scan the line A,B. The modulation ratio is essentially constant edge to edge, however. At 200-MHz modulation frequency, the time-resolved images are again almost-featureless as expected, but the phase gradient has now increased to about 7° as we scan the line A,B. Again, this occurs at an apparently constant modulation depth. The fact that the observed phase gradient direction is always found to align with the overall illumination axis indicates that a simple optical geometry explanation is in order. Because of the macroscopic dimension scale of these images and because the light is delivered to the sample from one side only at a defined angle (45°), there exists a substantial and easily calculatable optical pathlength difference between point A and point B, B being the nearest point to the illumination source (and least phase delayed in the images). This pathlength difference (about 29 mm) should equal a time gradient of about 95 ps edge to edge, or a 1.7° phase gradient at 50 MHz, increasing to 6.8° at 200 MHz. The modulation depth of the light should remain constant independent of whether the light delivery is "early" (point B) or "late" (point A). Thus both the observed modulation depth and the phase images are entirely reasonable and, far from indicating some peculiar nonuniformity in either gain depth or effective timing across the microchannel plate, offer us a very easy and direct check of the timing resolution of the FLIM system. This is achieved without recourse to any specific fluorescence samples and, at least for macroimaging, provides a convenient timing resolution test in a purely physical way independent of any sample photochemistry. It can therefore be concluded that the timing resolution of the FLIM instrument is better than 100 ps if such "weak" phase gradients can be directly seen, and provides the user with confidence that the instrument is performing satisfactorily. Specifically there are no falloffs in image intensifier modulation depth at the edges compared to the center of the imaged field even at frequencies as high as 200 MHz.

RESULTS AND DISCUSSION

One of the key properties expected from a FLIM time-resolved image is that not only should the image be independent of signal intensity, but it should report uniquely on fluorescence lifetime changes. In particular, it should be possible to see clearly whether changes in the steady-state intensity at any one pixel compared to any other involve either a lifetime change or a change in local emitter concentration or density. To demonstrate this key feature, the following "phantom" fluorescence

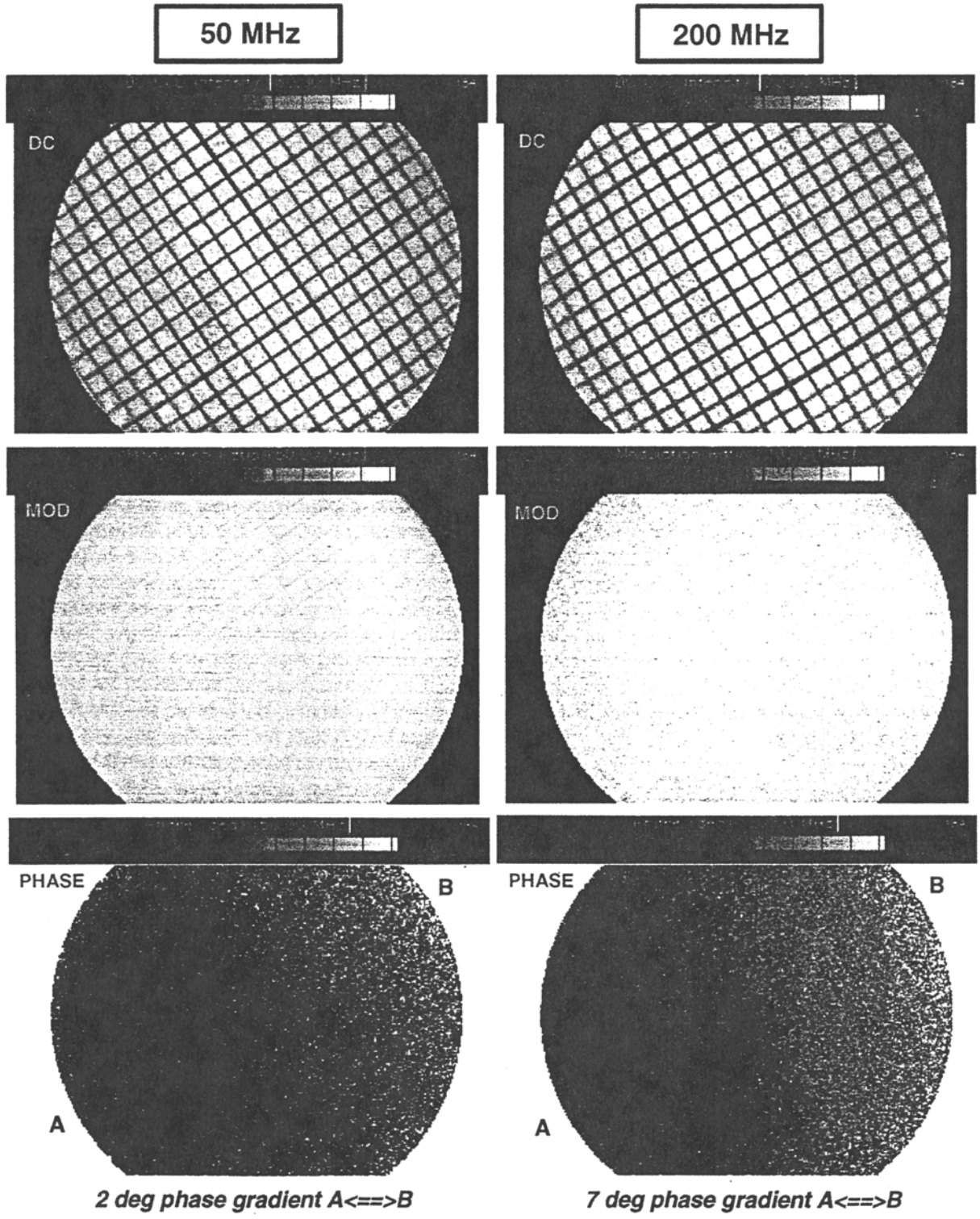

Fig. 3. Scattered light result images from a simple ruled graph paper target at 50 MHz (left column of images) and at 200 MHz (right column of images). The first row denotes the steady-state images (DC), the second row the modulation depth images (MOD), and the third row the phase images (PHASE). Each grid denotes 1/12 in., i.e., six squares per half-inch distance.

experiment was performed. The high-quantum yield, pH-independent, argon-ion laser-excitable, and water-soluble label BODIPY disulfonate was used as a trial fluorescer. This label was used on its own in dilute solution at various concentrations or at a single fixed label concentration but titrating the fluorescence lifetime using the classic collisional quencher potassium iodide (KI). A multimicrowell microscope slide was used as a sample carrier and a range of fluorescer concentrations 0–50 μM was added across the individual wells to form a concentration series. This sample should not show any significant lifetime changes well to well at these dye concentrations. A second well sample used the same label at a fixed 50 μM concentration, but with a graded concentration series of the quencher KI in the 0–200 mM range. This sample should show substantial lifetime reductions as the concentration of the quencher increases well to well, even though the real concentration of the label is in fact constant. The combined results of the concentration series and quenching series are shown in Fig. 4. Only the fluorescence emission images at 50 MHz are shown, the concentration series being the left-hand column of images and the quenching series the right-hand column. The top row in each column denotes the steady-state intensity images (DC), the middle row the modulation depth images (MOD), and the bottom row the phase images (PHASE). The numbers associated with each well in the DC concentration series denote label concentration in micromolar units and quencher concentration in millimolar units in the quenching series. Thus the steady-state intensity images show clear intensity contrast well to well in each series but for very different reasons. The concentration series represents a number-of-molecules gradient; the quenching series, a lifetime gradient at fixed label concentration. The time-resolved images (middle and bottom rows) clearly show neglible modulation depth or phase differences well to well in the concentration series, as indeed expected, but a clear gradient in these parameters for the quenching series. Thus FLIM clearly shows when lifetime reductions are causing drops in the steady-state intensity and, so, allow us to correct for such factors if we so wish. The most quenched (200 mM KI well) has the largest modulation depth and least phase-delayed values and so has the shortest fastest lifetime and hence the dimmest well in steady-state terms. The concentration-series phase values indicate a single average lifetime of about 5.5 ns for BODIPY disulfonate in distilled water over this concentration range taking the scattered light reference phase values into account (not shown). This value is in general agreement with literature lifetime values for the BODIPY fluorophore.[18]

In many industrial applications, the system or sample matrix in which fluorescence labels are required to be deployed will often be structurally complex, offering a range of microenvironments that could alter the emission lifetime of the extrinsic label in use. Often, these heterogeneous matrices or surfaces can exhibit fluorescence emission in their own right. Thus if we want to locate and potentially quantify a labeled macromolecule in such a system, not only will time-resolved imaging methods be very important but also they may offer some valuable discrimination power against such autofluorescence backgrounds. It is therefore important to characterize the emission lifetime properties of such background signals before choosing an extrinsic label, so that some clear separation can be achieved. One such autofluorescence example of interest to us at Unilever Research is that of dental enamel. This exhibits a strong intrinsic fluorescence which shows interesting steady-state intensity changes in regions of relative enamel disorganization. White-spot lesion areas, for example, show up as stronger scattering but weaker in intrinsic fluorescence areas compared to the surrounding sound enamel.[19–22] There are no clear spectral emission differences between such regions and their sound enamel surroundings, however.[23] A 50-MHz homodyne FLIM experiment was therefore performed on two human extracted premolar teeth, which both had white-spot lesion areas of varying clarity on their crowns, to see if there was any apparent lifetime differences between such lesion areas and their surroundings. Figure 5 shows the scattered light reference images (left column) and fluorescence emission images (right column) obtained at 50 MHz. The same meanings for the image rows as in Figs. 3 and 4 hold for the rows in Fig. 5. The most obvious white-spot lesion is seen on the crown of the lower tooth, marked WSL in Fig. 5. This scatters more than the surrounding enamel but has a lower apparent fluorescence signal. The junction between crown and root is also an area of abrupt change in sample topography, especially for the lower tooth shown, resulting in strong scattered light and apparent steady-state fluorescent signals. The time-resolved images (rows 2 and 3) show that there are no significant lesion contrasts for either modulation depth or phase in the scattered light images, but there is about a 10° phase increase in the phase fluorescence image (lower tooth lesion compared to surroundings) accompanied by a small increase in modulation depth. This translates to a clear lifetime reduction of about 0.5 ns for this lesion area compared to the surrounding sound enamel, the average crown enamel lifetime being about 2 ns. The modulation depth is clearly predicting a lower lifetime difference, which probably indicates that a more

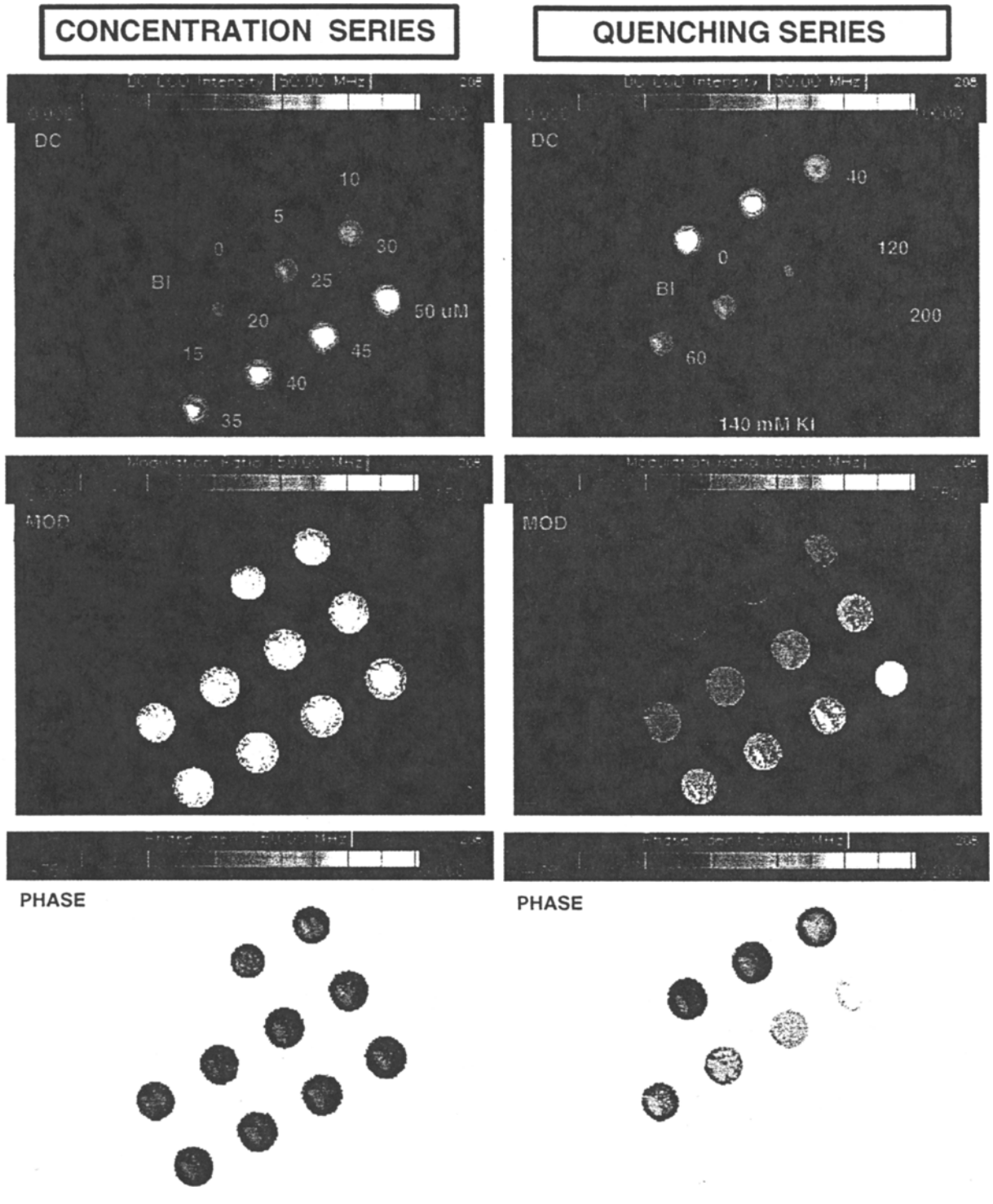

Fig. 4. Fluorescence emission result images at a 50-MHz modulation frequency. The left column of images denotes a concentration series of BODIPY disulfonate, 0–50 μM; the right column, a quenching series at a fixed BODIPY disulfonate concentration (50 μM), the quencher being KI in the range 0–200 mM. The microwell labeled Bl indicates an empty blank well; all other microwell numbers refer to either fluorophore or quencher concentration as appropriate. The row sequence and meaning are as given for Fig. 3.

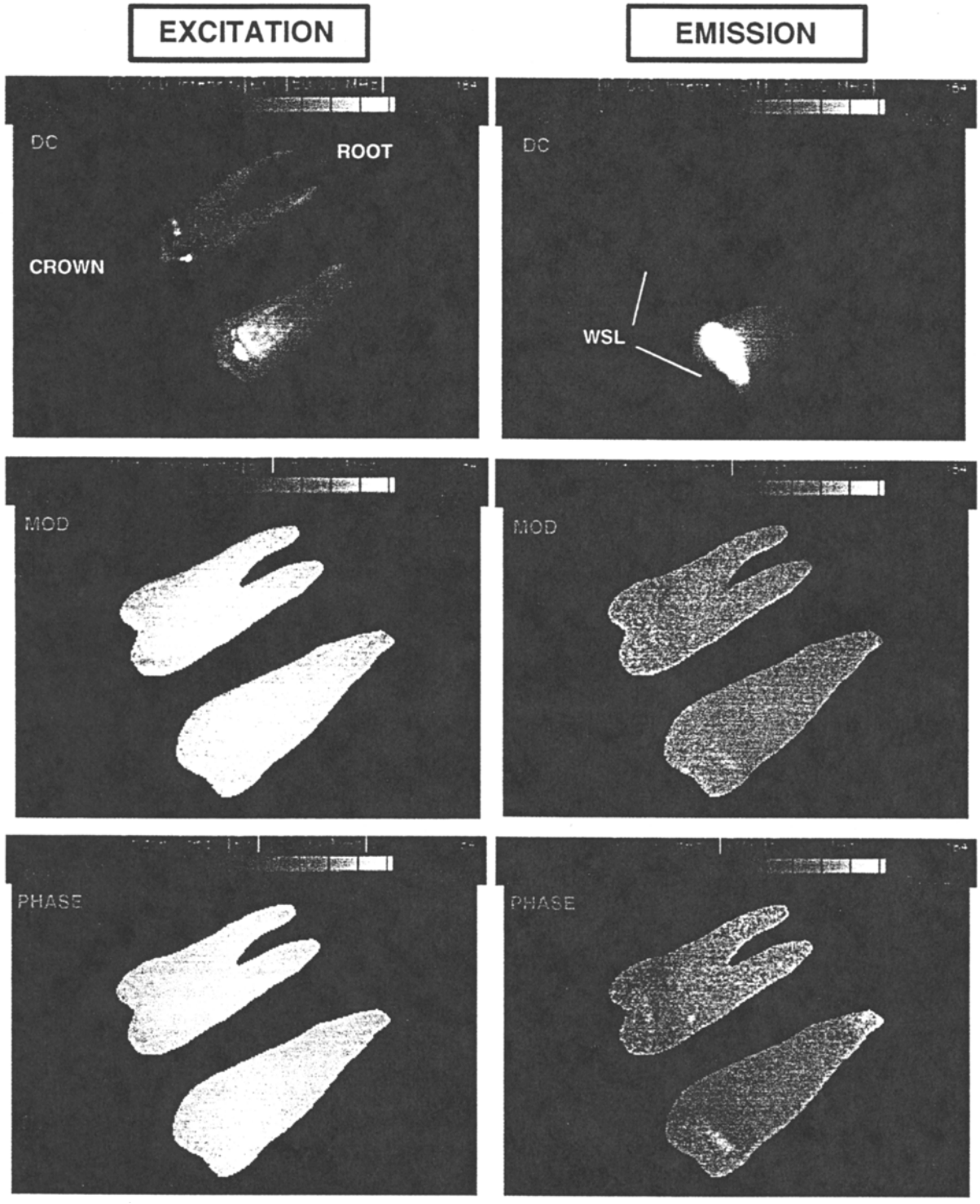

Fig. 5. Dental autofluorescence result images at a 50-MHz modulation frequency. The left column of images denotes the scattered light excitation stack images; the right column, the fluorescence emission images. The row sequence and meaning are as given for Fig. 3. WSL denotes clear white-spot lesion areas on the crown of each tooth.

complex decay law than a simple single exponential needs to be considered. Images at more than one modulation frequency would need to be acquired to clarify this point. These results are in general agreement with previous literature values using nonimaging time-resolved techniques.[20] Therefore it has been shown that one component in the steady-state contrast phenomenon of white-spot lesions is that of lifetime reduction of the unknown enamel emitter(s) in the lesion areas compared to the surrounding sound enamel. This may be of interest as regards early clinical detection of such lesion areas in the future.

CONCLUSIONS

A flexible wide-bandwidth fluorescence lifetime imaging instrument has been successfully constructed and tested. The key image intensifier operates with satisfactory modulation depth for the homodyne FLIM experiment, even up to a 200-MHz modulation frequency. No modulation depth falloffs are experienced at the edge of the imaging area relative to the center even at such high frequencies with this device. The very small additional phase delay due to light traveling to the far side of a macroscopic sample field away from the illumination point has been directly seen and indicates that the ultimate lifetime resolution of the system is no worse than about 100 ps. The instrument performs as expected as regards independence of steady-state signal intensity and with imaging contrast specifically for lifetime differences only. Dental enamel autofluorescence has also been investigated in a FLIM manner and 0.5-ns lifetime differences between white-spot lesions and their surrounding enamel have been clearly imaged. This forms one component explaining the white-spot lesion steady-state fluorescence contrast phenomenon.

ACKNOWLEDGMENTS

The author wishes to thank John Woolgar at EEV Ltd. for his considerable efforts in design and initial testing of the gain-modulatable image intensifier used in this work and Rob Treloar (Unilever Research) for ongoing support with PV-Wave programming tasks.

REFERENCES

1. J. R. Lakowicz and K. L. Berndt (1991) *Rev. Sci. Instrum.* **62**(7), 1727–1734.
2. J. R. Lakowicz, I. Gryczynski, H. Szmacinski, and K. Nowaczyk (1991) *SPIE* **1599**, 227–243.
3. R. M. Clegg, B. Fedderson, E. Gratton, and T. M. Jovin (1992) *SPIE* **1640**, 448–460.
4. T. W. J. Gadella, T. M. Jovin, and R. M. Clegg (1993) *Biophys. Chem.* **48**, 221–239.
5. C. G. Morgan, A. C. Mitchell, and J. G. Murray (1992) *J. Microsc.* **165**(1), 49–60.
6. C. G. Morgan, A. C. Mitchell, and J. G. Murray (1992) *Trends Anal. Chem.* **11**(1), 32–41.
7. T. Ni and L. A. Melton (1991) *Appl. Spectrosc.* **45**(6), 938–943.
8. K. Sasaki, M. Koshioka, and H. Masuhara (1991) *Appl. Spectrosc.* **45**(6), 1041–1045.
9. K. P. Ghiggino, M. R. Harris, and P. G. Spizzirri (1992) *Rev. Sci. Instrum.* **63**(5), 2899–3002.
10. E. P. Buurman, R. Sanders, A. Draaijer, H. C. Gerritsen, J. J. F. van Veen, P. M. Houpt, and Y. K. Levine (1992) *Scanning* **14**, 155–159.
11. D. W. Piston, D. R. Sandison, and W. W. Webb (1992) *SPIE* **1640**, 379–390.
12. C. Y. Dong, P. T. C. So, T. French, and E. Gratton (1995) *Biophys. J.* **69**, 2234–2242.
13. R. B. Thompson and J. R. Lakowicz (1993) *Anal. Chem.* **65**, 853–856.
14. R. Sanders, A. Draaijer, H. C. Gerritsen, P. M. Houpt, and Y. K. Levine (1995) *Anal. Biochem.* **227**, 302–308.
15. J. R. Lakowicz, H. Szmacinski, K. Nowaczyk, and M. L. Johnson (1992) *Cell Calcium* **13**, 131–147.
16. J. R. Lakowicz, H. Szmacinski, K. Nowaczyk, K. L. Berndt, and M. L. Johnson (1993) in O. S. Wolfbeis (Ed.), *Fluorescence Spectroscopy*, Springer, Berlin, pp. 129–146.
17. J. R. Lakowicz, H. Szmacinski, K. Nowaczyk, and M. L. Johnson (1992) *Proc. Natl. Acad. Sci. USA* **89**, 1271–1275.
18. J. Karolin, L. B. A. Johansson, L. Strandberg, and T. Ny (1994) *J. Am. Chem. Soc.* **116**, 7801–7806.
19. H. Bjelkhagen, F. Sundstrom, B. Angmar-Mansson, and H. Ryden (1982) *Swed. Dent. J.* **6**, 1–7.
20. F. Sundstrom, K. Fredriksson, S. Montan, U. Hafstrom-Bjorkman, and J. Strom (1985) *Swed. Dent. J.* **9**, 71–80.
21. T. Araki, E. Miyazaki, T. Kawata, and K. Miyata (1990) *Appl. Spectrosc.* **44**(4), 627–631.
22. U. Hafstrom-Bjorkman, F. Sundstrom, E. de Josselin de Jong, A. Oliveby, and B. Angmar-Mansson (1992) *Caries Res.* **26**, 241–247.
23. J. J. Birmingham, E. G. Mahers, and R. K. Chesters (1992) *J. Dent. Res.* **71**, A387.